Title

Direct 48 V to 6 V Automotive Hybrid Switched-Capacitor Converter with Reduced Conducted EMI

ISBN

9781665410816

Authors

Blackwell, Margaret E
Krishnan, Sahana
Ellis, Nathan Miles
et al.

Publication Date

2022-06-23

DOI

10.1109/compel53829.2022.9830026

2022 IEEE 23rd Workshop on Control and Modeling for Power Electronics (COMPEL), Tel Aviv, Israel, June 2022

Direct 48 V to 6 V Automotive Hybrid Switched-Capacitor Converter with Reduced Conducted EMI

M. E. Blackwell
S. Krishnan
N. M. Ellis
R. C. N. Pilawa-Podgurski

Direct 48 V to 6 V Automotive Hybrid Switched-Capacitor Converter with Reduced Conducted EMI

Margaret E. Blackwell, Sahana Krishnan, Nathan Miles Ellis, Robert C.N. Pilawa-Podgurski
Department of Electrical Engineering and Computer Sciences
University of California Berkeley

***Abstract*—With the rapid growth and development of high-density power converter topologies, including hybrid switched-capacitor converters, data-centers have seen a shift towards 48 V bus architectures for reduced transmission losses. In parallel, the automotive industry has similarly benefited from these advancements, with the proliferation of 48 V batteries allowing for reduced cable weight. However, the latter application space comes with additional challenges such as automotive-qualified component selection and the need to meet rigorous electromagnetic interference (EMI) standards. This work proposes a new interleaved-input, single-inductor Dickson converter with a high conversion ratio (8:1) for 48 V automotive applications. The impacts of operating frequency on efficiency and EMI performance are explored, as well as EMI mitigation techniques such as spread-spectrum frequency modulation (SSFM). A hardware prototype was built to demonstrate these concepts, and was characterized with respect to the CISPR 25, Class 5 EMI standards required for many automotive applications.**

I. Introduction

As consumption shifts towards more hybridized and fully electric vehicles (EVs), internal combustion engine (ICE) vehicles are starting to adopt 48 V batteries in place of the legacy 12 V battery, aligning themselves with EVs where 48 V may be used as an intermediary step-down from the high voltage battery. The use of a higher voltage bus decreases I^2R transmission losses and allows for lighter-weight cabling systems to be employed within the vehicle. The more power-hungry subsystems may be powered from a 48 V bus directly, instead of from a 12 V bus. Furthermore, the lower-voltage subsystems may be driven from a 48 V bus using high-density point-of-load (PoL) converters [1]–[5]: following similar trends to data-center power delivery [6]–[11], automotive power delivery can eliminate a conversion step by completely removing the 12 V intermediary bus. Current industry solutions for 48 V to PoL power conversion from companies like Vicor and EPC boast high efficiencies (upwards of 97%) [12], [13] and qualification for standards such as the CISPR 25, Class 5 electromagnetic interference (EMI) standard.

Fig. 1: Photograph of a 48 V to 6 V interleaved-input single-inductor Dickson converter built for demonstration of circuit operation as well EMI mitigation techniques.

In exploring 48V-to-PoL conversion and investigating the trade-offs between efficiency and EMI performance, this paper proposes an 8-to-1 hybrid Dickson switched-capacitor converter (Figs. 1 and 2). This topology is advantageous in this application space due to its interleaved high-side input and an inductor at the output that allows for complete soft-charging of the flying capacitors. Section II of this paper analyzes the converter operation and discusses its benefits and drawbacks. Section III explains the trade-offs of switching at and above resonance as these operational modes relate to efficiency and EMI performance. Section IV discusses the spread-spectrum frequency modulation (SSFM) EMI mitigation technique. Last, Section V includes details of the experimental prototype as well as measured efficiency and EMI results.

II. Interleaved-Input, Single-Inductor Dickson Converter

A new hybrid switched-capacitor (SC) topology (Fig. 2) proposed in this work combines several techniques that make this converter especially attractive for off-battery low-voltage automotive converters. As a variation on the hybrid Dickson converter [14], [15], this topology takes a similar approach to interleaving as the two-phase interleaved stacked-ladder in [16]. However, in this work's variation, the base topology is inherently interleaved with a single inductor on the output instead of two tank-configured inductors. While the interleaved stacked-ladder in [16] requires $4N$ switches for an $N:1$ conversion, the proposed topology only requires $2N+4$ and also eliminates the need for a distributed bypass capacitor column. Moreover, its capability for continuous forward conduction allows for regulation through selective phase insertion [17] without incurring increased circulating currents. The proposed interleaved-input, single-inductor Dickson converter has among the lowest normalized Volt-Amp switch-stress [18], and while its normalized passive volume is not as competitive as other hybrid SC topologies, its passive volume is still significantly smaller than ladder-type and conventional buck topologies, especially at higher conversion ratios [18].

The interleaved input of this Dickson-style converter allows charge to be transmitted from the high-side input V_{IN} during both switching phases despite using a single inductor; a feature unachievable with a single conventional buck where multiple converters (and inductors) must be interleaved. Subsequently the input filtering requirements are reduced (e.g. smaller input capacitance is needed), making this approach advantageous for

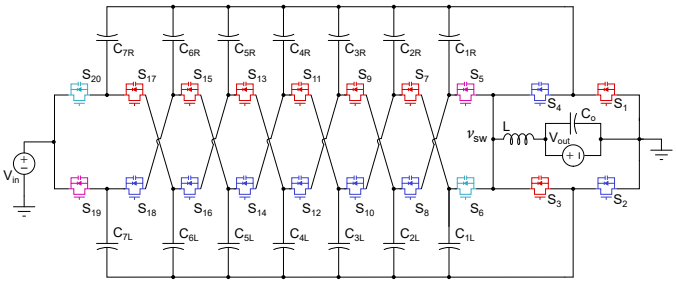

Fig. 2: Schematic of an 8-to-1 interleaved-input, single-inductor Dickson converter. Phase 1 (red), and Phase 2 (blue).

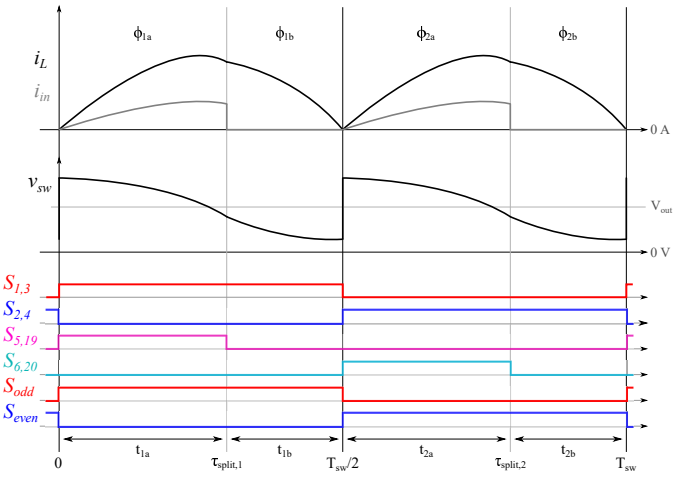

Fig. 3: Gate signals and key converter waveshapes (exaggerated for illustrative purposes) for the 8-to-1 interleaved-input, single-inductor Dickson converter employing split-phase operation.

applications, such as automotive, where designing a compact input filter is desired. In addition, the single inductor at the output acts as an EMI filter for the low-side output, while simultaneously providing a current path for soft-charging of the internal flying capacitors [17], resulting in very high passive component utilization.

Exemplar gating signals and corresponding converter operation waveforms for an 8:1 (N:1) interleaved-input, single-inductor Dickson converter are shown in Fig. 3 and equivalent circuits for each phase (and sub-phase) in Fig. 4. Assuming only two-phase operation is required, all odd-numbered switches ("bridge" switches S_1, S_3 and "string" switches $S_5 - S_{19}$) are turned "ON" during Phase 1 and all even-numbered switches ("bridge" switches S_2, S_4 and "string" switches $S_6 - S_{20}$) are turned "ON" during Phase 2. Due to this topology's interleaved symmetry, sizing flying capacitors such that $C_{xL} = C_{xR}$ for $x = 1 : N-1$, enforces Phase 1 (Fig. 4a) and Phase 2 (Fig. 4c) to have equivalent effective capacitance as seen by the inductor. Since the singular inductor at the output is engaged with an identical capacitor network during both phases, Phase 1 and Phase 2 are equivalent, thereby simplifying the analysis of this topology. Furthermore, with Phase 1 and Phase 2 being equivalent, this converter can operate with a 50% duty cycle between Phases 1 and 2. This implementation imposes a twice-frequency voltage ripple at

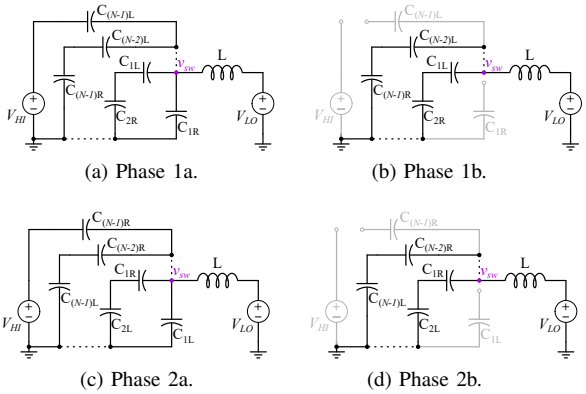

(a) Phase 1a. (b) Phase 1b.

(c) Phase 2a. (d) Phase 2b.

Fig. 4: Equivalent circuits for each sub-phase of an 8-to-1 Dickson converter, with split-phase switching sequence as ordered a-d: Phase 1a → Phase 1b → Phase 2a → Phase 2b.

the switch node and a current through the inductor which has a frequency twice that of the switching frequency.

There is, however, one caveat to maintaining soft-charging of the flying capacitors and subsequent high passive utilization: split-phase operation is required. Detailed in [19], split-phase operation describes the introduction of sub-phases within the two main switching phases to ensure soft-charging of the flying capacitors through the output inductor. Without these additional switching states, large current spikes occur at phase transitions due to mismatched loop voltages. These hard-charging events have a negative impact on efficiency, passive utilization, and EMI performance. In this work, to satisfy voltage loops at phase transitions, the sub-phases 1b (Fig. 4b) and 2b (Fig. 4d) are inserted between the transition from Phase 1a to 2a and from 2a to 1a, respectively. Since capacitors $\{C_{1R}, C_{7L}\}$ and $\{C_{1L}, C_{7R}\}$ are not series-connected to other capacitors during Phase 1a and Phase 2a respectively, these capacitors accrue charge more quickly than the other flying capacitors (assuming all capacitors are equally sized). Switches S_5 and S_{19} (Phase 1b) and Switches S_6 and S_{20} (Phase 2b) turn "OFF" to remove capacitors $\{C_{1R}, C_{7L}\}$ and $\{C_{1L}, C_{7R}\}$ respectively from the circuit before they are reconnected in a different configuration for the following phase. Satisfying the voltage loops requires correct timing of the "b-phase" durations and placement within the primary phases 1 and 2. Owing to the requirement for split-phase switching, input switches S_{19} and S_{20} turn "OFF" towards the end of primary Phases 1 and 2, respectively, thereby disconnecting the input source. As such, while the input current is not fully continuous throughout each period, there is still significant improvement over a single-ended topology, where the input current would be zero for the entirety of one phase.

III. Choice of Operation Frequency

In this work, we explore the trade-offs between different operation ranges, and specifically, how the choice of switching frequency impacts efficiency and EMI performance. Two regions of frequency bands for exploration are at-resonant ($f_{sw}/f_0 = 1$ in Fig. 5) and above-resonant ($f_{sw}/f_0 > 1$ in Fig. 5 [20]) frequencies. Operating at resonance means that the converter can achieve zero current switching (ZCS)

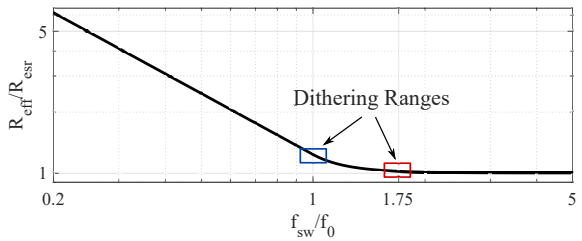

Fig. 5: Effective output resistance versus frequency of an exemplary **two-phase** resonant hybrid SC converter operating in CCM (red) and at resonance, i.e. the boundary between CCM and DCM (blue) [20].

on all switches, except for the split-phase switches S_5, S_6, S_{19}, and S_{20}. ZCS can reduce switching losses as well as switching noise, improving efficiency and EMI. However, resonant operation has larger RMS current when compared to operating above resonance, leading to larger conduction losses. Furthermore, above-resonant operation often has increased switching losses due to the increased switching frequency. With regards to efficiency, at-resonant operation may be better at lighter loads, where switching losses are a larger portion of the losses, whereas above-resonant operation may be better at heavier loads where conduction losses dominate. Operation in each of these frequency bands is analyzed in Section V.

IV. EMI Mitigation Technique

EMI is a challenge in any switching converter, where switching events can create unwanted noise that must be strategically mitigated. Spread-spectrum frequency modulation (SSFM) is a control technique that uses a variable switching frequency to reduce conducted EMI [21]–[24]. To implement this, the converter's periodic switching frequency can be modulated, or dithered, and therefore spread out the original energy of each harmonic about a specified frequency band. This provides a wider spectrum with lower peak amplitudes.

There are many modulation schemes for SSFM, a few of which are described in [21]–[24]. The fundamental parameters for the frequency modulation profiles are:

f_c	Center frequency, or nominal frequency about which the switching frequency is dithered.
Δf_c	Step size of frequency dithering.
$T_m = \frac{1}{f_m}$	Period/frequency of modulation profile.
A_m	Maximum deviation of switching frequency from center frequency, f_c.

The three modulation schemes – right-triangular, triangular, sinusoidal – tested in this work are shown in Fig. 6. The EMI effects of changing parameters Δf_c, f_m, and A_m are presented in Section V.

Moreover, implementing SSFM can have impacts on efficiency. Fig. 5 plots the effective output resistance [20] of an example two-phase resonant converter operating in discontinuous conduction mode (DCM) for $f_{sw}/f_0 < 1$ and continuous conduction mode (CCM) for $f_{sw}/f_0 > 1$. For simplicity of presentation, this plot does not account for hard-charging/split-phase operation nor for forced DCM (which the converter in this work uses), which would introduce additional peaks and valleys at frequencies much below the resonant frequencies. Because this work focuses on at- and above-resonant operation, the simplified output resistance plot of Fig. 5 is a good reference in analyzing the impacts of SSFM on this work's converter operation.

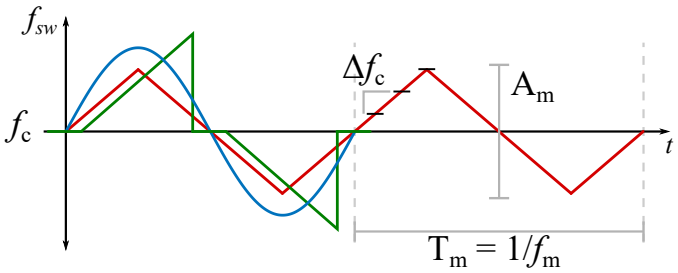

Fig. 6: Modulated switching frequency over time and key parameters for various SSFM schemes: right-triangle (green), triangle (red), and sinusoidal (blue).

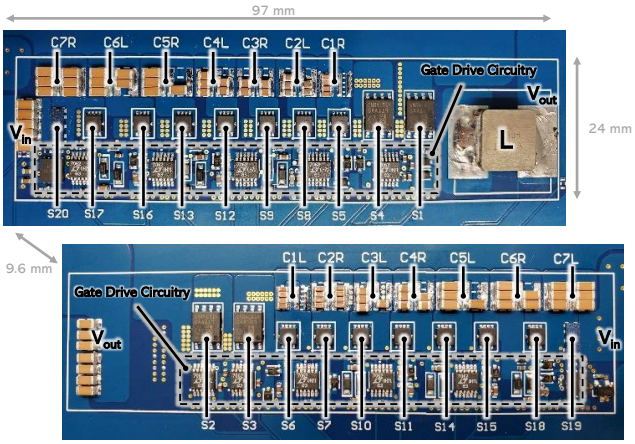

Fig. 7: Image of prototype board with key components labeled.

As the switching frequency becomes greater than the resonant frequency, the effective output resistance, R_{eff}, approaches its limit, R_{esr}, which is the effective series resistance of the power components, and represents the lowest possible output resistance. Consequently, operating with a center frequency sufficiently above resonance and with a relatively small dithering band, the losses for the converter remain relatively constant, for example the band around $f_{sw}/f_0 = 1.75$. However, with a center frequency close to the resonant frequency, even a very small dithering band gives non-negligible variation in R_{eff} and therefore converter efficiency. The EMI benefits from SSFM may not outweigh the negative impacts on efficiency when operating near resonance, but may be significant for above-resonant operation.

V. Experimental Prototype

An 8-to-1 discrete hardware prototype was constructed to verify operation as well as to explore efficiency and EMI trade-offs of the proposed interleaved-input single-inductor Dickson converter (Fig. 7). The experimental prototype, measuring

TABLE I: Component Listing of the Hardware Prototype

Component		Mfr. & Part Number	Parameters
Dickson Power Stage			
Start-up Switches	S_{19} - S_{20}	EPC EPC2206	GaN, 80 V, 2.5 mΩ
String Switches	S_5 - S_{18}	ON Semiconductor NVTFS002-N04CL	Si, 40 V, 3.5 mΩ
Bridge Switches	S_1 - S_4	Infineon IAUC100-N04S6L014	Si, 40 V, 1.4 mΩ
Flying Capacitors	C_{1x}, C_{2x}	Murata GRT188R61H225KE13	X5R, 50 V, 2.2 μF (x5, x6)
	C_{3x}, C_{4x}	TDK CGA4J3X5R1H475K125AB	X5R, 50 V, 4.7 μF (x3, x4)
	C_{5x}, C_{6x}, C_{7x}	TDK CGA5L3X5R1H685K160AB	X5R, 50 V, 6.8 μF (x4, x5, x6)
Inductor	L	Vishay Dale IHLP4040DZERR19MA1	0.19 μH, 90 A I_{sat}
Gate Drive			
GaN Driver		Texas Instruments LM5113QDPRRQ1	90 V, high and low-side
LDO		Microchip MCP1792T-5002H	5.0 V, 100 mA
Si Gate Driver (and Charge Pump)		Analog Devices Inc. LTC7062IMSE	Dual high-side driver
Bootstrap Diodes		Nexperia PMEG6002EJ,115	Schottky, 60 V, 200 mA
Charge Pump Diodes		Diodes Inc. PD3S230L-7	Schottky, 30 V, 2 A
Charge Pump Capacitors		Murata GRT188R61H225ME13D	X5R, 50 V, 2.2 μF
Controller Board			
FPGA		Terasic Inc. P0466	DE10-Lite, Max10 FPGA

TABLE II: Converter Operating Parameters

Parameter	Value	Units
V_{in}	48	V
V_{out}	6	V
$P_{out,max}$	120	W
f_{sw}	50-200	kHz
f_{res}	81	kHz

24 mm x 97 mm x 9.6 mm, utilizes mixed switch technologies (both Si and GaN) to optimize for on-state resistance ($R_{DS_{on}}$), drain-to-source voltage (V_{DS}), and gate charge (Q_G). Both Cascaded Bootstrap and Gate-Driven Charge Pump methods [25] are used for bootstrapping in the gate drive power circuit. Furthermore, all components (Table I) on the board are automotive-qualified so as to adhere to the Automotive Electronics Council (AEC) standards. Inductor and capacitor values were chosen to give a resonant switching frequency of 81 kHz, a frequency whose fundamental is below the lowest relevant EMI frequency band. Table II defines the operating parameters for this prototype.

A. *Efficiency Measurements*

As discussed above, the mode of operation can impact the efficiency of the converter, especially when comparing resonant (i.e. ZCS) operation with above-resonant operation (i.e. faster switching). Efficiency curves for a range of frequencies around resonance and faster than resonance are presented to compare switching frequency effects on power loss. Additionally, efficiencies were recorded for various switching frequencies with and without utilizing SSFM schemes to demonstrate how SSFM impacts (or does not impact) efficiency.

Fig. 8 depicts static (meaning no SSFM is employed) efficiency curves for several switching frequencies around

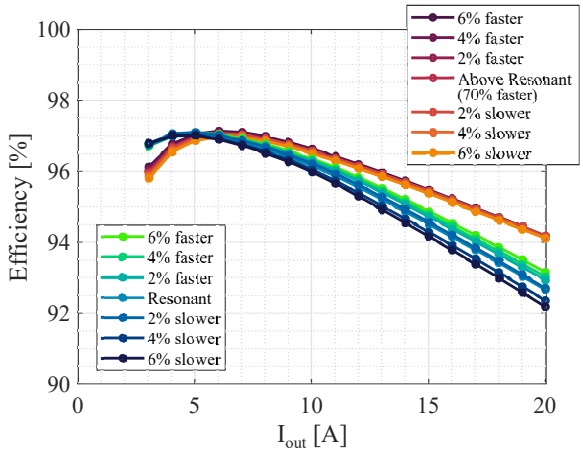

Fig. 8: Static efficiency plots for frequency bands near resonant and above-resonance operation at 48 V input and un-regulated 6 V output.

resonance and around the frequency 70% faster than resonance. The spread of efficiency lines for resonant and above-resonant operation agree with behavior estimations in Fig. 5: for a frequency spectrum around the resonant frequency, the efficiency varies with frequency. However, for operation above resonance, the converter losses are relatively constant with changes in frequency.

Moreover, as expected, resonant operation and its lower switching losses yield better light load efficiency, while the reduced RMS currents of above-resonant operation yields higher efficiency at heavy load, where conduction losses dominate.

Furthermore, efficiency versus load curves (Fig. 9) were taken for converter operation at various switching frequencies without SSFM as well as operation utilizing different SSFM schemes, as described in Table III. For higher frequency SSFM modulation, a center frequency, f_c, of 70-75 % faster than resonance was selected. For this circuit implementation, 75% faster than resonance corresponds to 143 kHz. This frequency

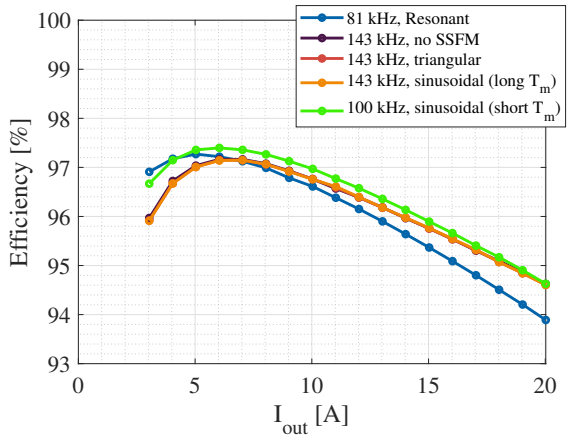

Fig. 9: Efficiency plots for 48 V input, resonant and above-resonance operation with and without SSFM.

was chosen so that the fundamental frequency component is kept below the lowest frequency band of CISPR 25 regulations, Table IV.

Here, the peak efficiency is 97.27% for resonant operation at 5 A, whereas, the peak efficiency is about 97.16% for all of the 143 kHz operation modes at a load of 6 A. For operation only slightly faster than resonance, 100 kHz (about 20% faster than resonance), the peak efficiency at 5 A for SSFM Mode 5 is 97.35%. At light loads, the at-resonance efficiency exceeds above-resonance efficiency, whereas, at heavy loads, the efficiency for the above-resonance case exceeds that of the resonant case. This trend results due to conduction loss dominating over switching loss at heavy load, and so the gains seen by resonant-ZCS do not outweigh the reduction in RMS currents seen at higher switching frequencies. Looking at the three different SSFM schemes represented in Fig. 9, the peak efficiency of the 100 kHz case with sinusoidal SSFM exceeds that of both the 143 kHz cases with SSFM. Among the three different efficiency curves for 143 kHz presented here, it can be seen that employing SSFM at frequencies much faster than resonance does not affect the efficiency significantly as all three curves for 143 kHz are practically indistinguishable, regardless of the spread-spectrum modulation scheme. However, the efficiency for 143 kHz operation differs from that of 100 kHz operation even though both of these frequencies are higher than resonance. The difference between these two center frequencies and why the losses are different is because 100 kHz (at only 20% faster than resonance) falls much closer to the elbow of the output impedance versus frequency plot in Fig. 5. This means that the output impedance and therefore losses are slightly more correlated with changes in frequency. From looking at the efficiency data for these several modes of operation, we can see the efficiency trends of operation at and above resonance, as well as the negligible impact of employing SSFM schemes on efficiency. The next section explores effects these different operational modes have on EMI performance.

TABLE III: Definition of Converter Modes of Operation

Mode 1	81 kHz, Resonant
Mode 2	143 kHz, no SSFM
Mode 3	143 kHz, triangular SSFM, Δf_c = 3.24 kHz, f_m = 1.43 kHz, and A_m = 16.19 kHz
Mode 4	143 kHz, sinusoidal SSFM with long T_m, f_m = 446.88 Hz, and A_m = 4.78 kHz
Mode 5	100 kHz (or 143 kHz), sinusoidal SSFM with short T_m, f_m = 625 Hz (or 893.75 Hz), and A_m = 35.5 kHz (or 7.50 kHz)
Mode 6	143 kHz, right triangle SSFM, Δf_c = 752.5 Hz, f_m = 1.43 kHz, and A_m = 2.26 kHz

TABLE IV: Conducted Noise Limits for CISPR 25, Class 5 EMI Standards

Band	Frequency (MHz)	Peak Limit (dBμV)
LW	0.15-0.3	70
MW	0.53-1.8	54
SW	5.9-6.2	53
FM	76-108	38
TV	41-88	34
CB	26-28	44
VHF I	30-54	44
VHF II	68-87	38

B. EMI

In addition to low power loss, another key requirement for automotive converters is EMI emissions below standardized values. Here, we measure the EMI at the input side which is connected to the 48 V bus because the bus voltage should be stiff and without excess noise injected. At the low side port, there are other PoL converters downstream and therefore, noise is of a slightly lower concern than the input port. Figures 10-11 serve to make a comparison of spread-spectrum versus non-SSFM EMI performance at an input voltage of 48 V, an (unregulated) output voltage of 6 V, and a load current of 20 A. These noise measurements were taken in a laboratory, pre-compliance semi-shielded environment using the *Tektronix RSA306b*. A comparison between Mode 1 and Mode 2, as well as between Mode 1 and Mode 3, from Table III are presented. Both Common Mode (CM) and Differential Mode (DM) noise is shown for each case. It should be noted that in this work, we are interested in analyzing the raw EMI emissions from the converter, so no dedicated EMI filter was employed in these measurements. In the Figs. 10 and 11, the blue trace corresponds to resonant operation with no SSFM employed and acts as a reference within each of the plots to compare the EMI performance of each SSFM mode.

The horizontal lines on the plots denote the CISPR 25, Class 5 standard conducted emissions limits [26] (Table IV). It can

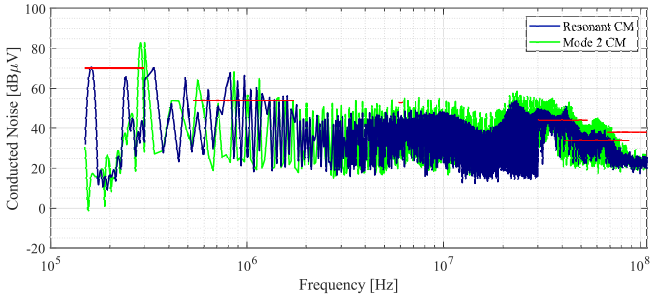

(a) Common mode (CM) conducted emissions.

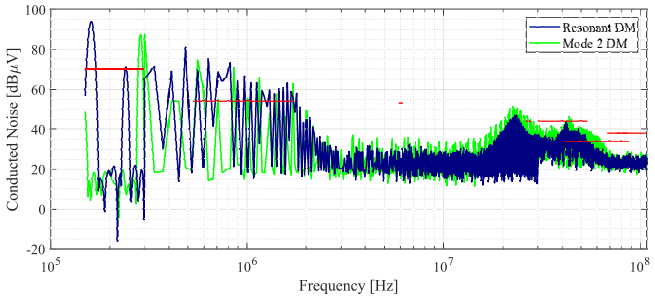

(b) Differential mode (DM) conducted emissions.

Fig. 10: Conducted emissions for 81 kHz (blue) and 143 kHz (green) with no SSFM, Modes 1 and 2, respectively, at an input voltage of 48 V, an (unregulated) output voltage of 6 V, and a load current of 20 A.

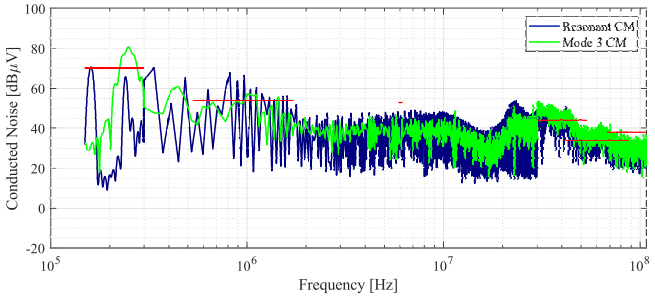

(a) Common mode (CM) conducted emissions.

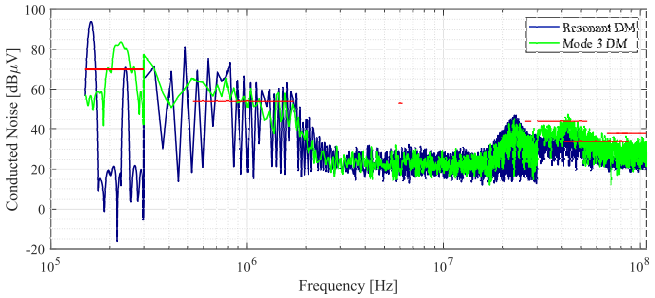

(b) Differential mode (DM) conducted emissions.

Fig. 11: Conducted emissions for 81 kHz (blue) with no SSFM and 143 kHz (green) with triangle SSFM, Modes 1 and 3, respectively, at an input voltage of 48 V, an (unregulated) output voltage of 6 V, and a load current of 20 A.

be seen that the peaks occur around 162 kHz and 286 kHz for at resonance and above resonance, respectively. These frequencies are consistent with twice the switching frequency (i.e. the frequency of the inductor current and switch-node voltage).

First, a comparison of resonant and above-resonant EMI performance is presented in Fig. 10 without the use of SSFM. For both CM and DM, the noise profiles are similar. However, the location and magnitude of peaks differ. Due to the soft-switching capability of the resonant operating mode, much of the switching noise can be eliminated, reducing the conducted noise from the converter. For CM noise, the resonant case shows noise levels only slightly above the required limits for the lowest pertinent frequency range. Comparatively, the above-resonant operating mode, while having better efficiency at this voltage and loading condition, has higher CM noise peaks (particularly at the lower frequency bands) without employing any SSFM than does the resonant case. Similar to the CM measurements, DM noise for the resonant case shows lower levels than the above-resonant case for a majority of the frequency bands. Despite generally lower peaks, resonant operation has higher noise levels in the LW band than the above-resonant case. These noise measurements in conjunction with the efficiency data discussed above indicate that there is a clear efficiency and EMI tradeoff between operating at and above resonance.

For the prototype in this work, the Common Mode peaks are generally lower than the Differential Mode peaks. Due to the switched-capacitor nature of the interleaved-input, single inductor hybrid Dickson topology, the converter has low voltage swing on the switch-node and throughout the circuit, leading to lower Common Mode noise. On the contrary, Differential Mode noise is heavily dependent on the current through the converter. Having several current paths and many capacitor branches, as this topology has, can correlate to larger current loops. Furthermore, the impact of larger current loops will be exacerbated at increasing load and with higher current ripple.

Owing to the requirement of split-phase switching, which results in the input voltage being disconnected from the circuit within each phase, the current ripple at the input source is non-zero. This leads to greater DM noise. Despite the impossibility of eliminating the input current ripple, clever circuit configuration (e.g. the implementation of an interleaved-input in this work) serves to reduce this source of DM noise as compared to a single-ended topology.

As showcased in the previous section, one advantage of operating above resonance is the invariability of efficiency with changing switching frequency. To take advantage of this feature, we can implement SSFM to potentially improve the EMI performance of this converter when it is operating above resonance. This is in an effort to make above-resonance noise levels more comparable to resonant noise levels. Fig. 11 and Table V show conducted emissions plots and related peak-to-limit data, respectively, for Mode 3 (Table III). For both the CM and DM cases, the noise level profile in the middle range of frequencies is noticeably smaller with triangle SSFM employed versus resonant operation with no SSFM. Addition-

TABLE V: CM and DM Noise Peaks for Various Modes of Operation

Mode	Band	Peak-to-Limit %	
		CM	DM
Mode 1	LW	0.86	34.2
	MW	25.7	38.9
	VHF I	15.6	-2.95
Mode 2	LW	17.1	25.3
‘	MW	26.5	38.0
	VHF I	27.0	5.41
Mode 3	LW	15.2	19.2
	MW	6.10	21.2
	VHF I	21.9	7.93
Mode 4	LW	23.7	23.8
	MW	31.8	37.3
	VHF I	26.4	5.41
Mode 5	LW	11.7	25.7
(143kHz)	MW	21.2	34.8
	VHF I	28.6	5.50
Mode 6	LW	17.6	23.3
	MW	18.2	38.2
	VHF I	22.9	-7.43

ally, the peaks are more spread out indicating the conversion of a narrower and taller peak into a wider and shorter one, the key premise of SSFM. In addition to providing lower losses at heavier loads, operating above resonance allows for the implementation of SSFM without a significant impact on efficiency, but with a clear benefit for EMI performance.

While only comparisons between Modes 1, 2 and 3 are discussed in detail here, Table V contains peak-to-limit percentages for each remaining SSFM mode outlined in Table III. Even though there is no definitive ‘best’ modulation scheme, for this prototype at this loading condition, the overall trend suggests that the more effective SSFM methods for reducing conducted emissions have a shorter modulation period, T_m, larger frequency step size, Δf_c, and larger maximum frequency deviation, A_m. Moreover, though several schemes for frequency dithering to spread the noise spectrum are presented here, these are only a small subset of the many schemes possible to help reduce conducted EMI.

Aside from implementing SSFM, strategic frequency placement, as well as an EMI filter can be used for EMI mitigation. When it comes to improving EMI at resonant operation, we can choose inductor and capacitor values that correspond to a lower resonant frequency such that not only is the fundamental component below 150 kHz (the lower end of the LW Band), but that the 2xf_{res} peak is as well. Another option for frequency manipulation would be to have the lower harmonics (fundamental or second) occur between the LW and MW frequency bands, avoiding the CISPR limits.

Furthermore, passive EMI filters can be designed to target peaks at specific frequencies, and therefore reduce conducted noise even further. For this topology, because the power inductor is directly connected to the output, it acts as a filter to the low-side port. However, to filter noise at the high-side port, a discrete EMI filter can be placed at the front end of the power converter. For this additional filter, passive components are selected to filter out specific frequency harmonics: where the noise peaks are occurring. Typically, the different conducted noise peaks appear at harmonics of the switching frequency. However, due to the requirement of split-phase switching (having switching transitions within a phase), the positioning of the peaks is more complicated than a simple multiple of the switching frequency. In this instance, having preliminary EMI measurements as presented here informs the design of the EMI filter. Furthermore, realizing the impact SSFM has on the location of the peaks is also necessary for a multi-faceted approach to mitigating and filtering out conducted emissions.

VI. Conclusion

Power conversion from the 48 V bus to PoL in automotives requires high efficiency and qualification for EMI standards. However, there are trade-offs between achieving these performance standards, which are informed by the analysis of at resonant and above-resonant operation presented here. This paper discusses the theory and construction of an 8-to-1 hybrid Dickson switched-capacitor converter for automotive systems. The topology testing focuses on achieving low EMI and high efficiency by utilizing an interleaved input, as well as frequency modulation techniques. In this work, the efficiency benefits of operating at resonance for light load, but above resonance (for reduced RMS currents and conduction losses) at heavier load were demonstrated. Additionally, several spread-spectrum frequency modulation schemes were compared for both efficiency and EMI performance. Dithering the frequency around a point higher than the resonant frequency has little impact on the efficiency, however, the benefits of SSFM on conducted EMI are evident. Specifically, triangular modulation, greatly flattens out the peak noise for both CM and DM EMI, which will reduce the amount of filtering required to meet CISPR 25, Class 5 requirements.

VII. Acknowledgments

The authors gratefully acknowledge support for this work in part from the National Science Foundation Graduate Research Fellowship Program under Grant No. DGE-1752814.

References

[1] F. Bez, G. Bonanno, L. Corradini, and C. Garbossa, “Control Technique for Reliable Operation of the Synchronous Series Capacitor Tapped Inductor Converter,” *IEEE Transactions on Power Electronics*, vol. 34, no. 8, pp. 8150–8161, 2019.

[2] Y. Naeimi and A. Huang, “Design and Optimization of High Conversion Ratio Quasi Square Wave Buck Converters,” in *2017 IEEE 5th Workshop on Wide Bandgap Power Devices and Applications (WiPDA)*, Oct. 2017, pp. 148–152.

[3] M. Ashourloo, V. R. Namburi, G. V. Piqué, J. Pigott, H. J. Bergveld, A. E. Sherif, and O. Trescases, “Decentralized Quasi-Fixed-Frequency Control of Multiphase Interleaved Hybrid Dickson Converters for Fault-Tolerant Automotive Applications,” *IEEE Transactions on Power Electronics*, vol. 35, no. 7, pp. 7653–7663, 2020.

[4] V. R. Namburi, M. Ashourloo, and O. Trescases, "Fast Transient Response of GaN-Based Hybrid Dickson Converter using Quasi-Fixed-Frequency Control for 48-V-to-1-V Direct Conversion in Automotive Applications," in *2020 IEEE Applied Power Electronics Conference and Exposition (APEC)*, 2020, pp. 33–40.

[5] M. Ashourloo, V. R. Namburi, G. V. Piqué, J. Pigott, H. J. Bergveld, A. E. Sherif, and O. Trescases, "17.2 A Masterless Fault-Tolerant Hybrid Dickson Converter with 95.3% Peak Efficiency 20V-to-60V Input and 3.3V Output for 48V Multi-Phase Automotive Applications," in *2021 IEEE International Solid- State Circuits Conference (ISSCC)*, vol. 64, 2021, pp. 258–260.

[6] Y. Li, X. Lyu, D. Cao, S. Jiang, and C. Nan, "A 98.55% Efficiency Switched-Tank Converter for Data Center Application," *IEEE Transactions on Industry Applications*, vol. 54, no. 6, pp. 6205–6222, 2018.

[7] J. Baek, P. Wang, S. Jiang, and M. Chen, "LEGO-PoL: A 93.1% 54V-1.5V 300A Merged-Two-Stage Hybrid Converter with a Linear Extendable Group Operated Point-of-Load (LEGO-PoL) Architecture," in *2019 20th Workshop on Control and Modeling for Power Electronics (COMPEL)*, 2019, pp. 1–8.

[8] Z. Ye, Y. Lei, and R. C. N. Pilawa-Podgurski, "The Cascaded Resonant Converter: A Hybrid Switched-Capacitor Topology With High Power Density and Efficiency," *IEEE Transactions on Power Electronics*, vol. 35, no. 5, pp. 4946–4958, 2020.

[9] Z. Ye, R. A. Abramson, and R. C. N. Pilawa-Podgurski, "A 48-to-6 V Multi-Resonant-Doubler Switched-Capacitor Converter for Data Center Applications," in *2020 IEEE Applied Power Electronics Conference and Exposition (APEC)*, 2020, pp. 475–481.

[10] R. A. Abramson, Z. Ye, and R. C. Pilawa-Podgurski, "A High Performance 48-to-8 V Multi-Resonant Switched-Capacitor Converter for Data Center Applications," in *2020 22nd European Conference on Power Electronics and Applications (EPE'20 ECCE Europe)*, 2020, pp. 1–10.

[11] Y. Zhu, T. Ge, Z. Ye, and R. C. Pilawa-Podgurski, "A Dickson-Squared Hybrid Switched-Capacitor Converter for Direct 48 V to Point-of-Load Conversion," in *2022 IEEE Applied Power Electronics Conference and Exposition (APEC)*, 2022, pp. 1272–1278.

[12] Vicor, "30 – 60VIN ZVS Buck Regulator (PI352x-00)," Online, Retrieved April 2nd 2022. [Online]. Available: https://www.vicorpower.com/documents/datasheets/ds_PI352x-00.pdf

[13] Efficient Power Conversion, "How to Design a 1.5 kW 48 V/12 V Bi-Directional Power Module with AEC Qualified eGaN® FETs," Online, Retrieved April 2nd 2022. [Online]. Available: https://epc-co.com/epc/DesignSupport/ApplicationNotes.aspx

[14] J. Dickson, "On-Chip High-Voltage Generation in MNOS Integrated Circuits Using an Improved Voltage Multiplier Technique," *Solid-State Circuits, IEEE Journal of*, vol. 11, no. 3, pp. 374–378, Jun 1976.

[15] Y. Lei, "High-Performance Power Converters Leveraging Capacitor-Based Energy Transfer," Ph.D. dissertation, University of Illinois at Urbana-Champaign, 2017.

[16] P. H. McLaughlin, P. A. Kyaw, M. H. Kiani, C. R. Sullivan, and J. T. Stauth, "A 48-V:16-V, 180-W Resonant Switched-Capacitor Converter With High-Q Merged Multiphase LC Resonator," *IEEE Journal of Emerging and Selected Topics in Power Electronics*, vol. 8, no. 3, pp. 2255–2267, 2020.

[17] Y. Lei and R. Pilawa-Podgurski, "Soft-charging Operation of Switched-capacitor DC-DC Converters with an Inductive Load," in *The Applied Power Electronics Conference and Exposition (APEC), 2014 IEEE*, 2014.

[18] Z. Ye, S. Sanders, and R. C. N. Pilawa-Podgurski, "Modeling and Comparison of Passive Component Volume of Hybrid Resonant Switched-Capacitor Converters," *IEEE Transactions on Power Electronics*, 2022.

[19] Y. Lei, R. May, and R. Pilawa-Podgurski, "Split-Phase Control: Achieving Complete Soft-Charging Operation of a Dickson Switched-Capacitor Converter," *IEEE Transactions on Power Electronics*, vol. 31, no. 1, pp. 770–782, 2016.

[20] C. Schaef, J. Rentmeister, and J. T. Stauth, "Multimode Operation of Resonant and Hybrid Switched-Capacitor Topologies," *IEEE Transactions on Power Electronics*, vol. 33, no. 12, pp. 10 512–10 523, Dec 2018.

[21] D. Gonzalez, J. Balcells, A. Santolaria, J.-C. Le Bunetel, J. Gago, D. Magnon, and S. Brehaut, "Conducted EMI Reduction in Power Converters by Means of Periodic Switching Frequency Modulation," *IEEE Transactions on Power Electronics*, vol. 22, no. 6, pp. 2271–2281, 2007.

[22] O. Trescases, G. Wei, A. Prodic, and W. T. Ng, "An EMI Reduction Technique for Digitally Controlled SMPS," *IEEE Transactions on Power Electronics*, vol. 22, no. 4, pp. 1560–1565, 2007.

[23] R. Gamoudi, D. Elhak Chariag, and L. Sbita, "A Review of Spread-Spectrum-Based PWM Techniques—A Novel Fast Digital Implementation," *IEEE Transactions on Power Electronics*, vol. 33, no. 12, pp. 10 292–10 307, 2018.

[24] D. Yan and D. B. Ma, "An Automotive-Use Battery-to-Load GaN-Based Switching Power Converter With Anti-Aliasing MR-SSM and In-Cycle Adaptive ZVS Techniques," *IEEE Journal of Solid-State Circuits*, vol. 56, no. 4, pp. 1186–1196, 2021.

[25] Z. Ye, Y. Lei, W.-C. Liu, P. S. Shenoy, and R. C. N. Pilawa-Podgurski, "Improved Bootstrap Methods for Powering Floating Gate Drivers of Flying Capacitor Multilevel Converters and Hybrid Switched-Capacitor Converters," *IEEE Transactions on Power Electronics*, vol. 35, no. 6, pp. 5965–5977, 2020.

[26] International Electrotechnical Commission (IEC), "CISPR 25 Vehicles, Boats and Internal Combustion Engines – Radio Disturbance Characteristics – Limits and Methods of Measurement for the Protection of On-Board Receivers," Oct. 2016.